Design and implementation of distributed ultra-high temperature sensing system with a single crystal fiber

Bo Liu*, Michael P. Buric, Benjamin T. Chorpening, Zhihao Yu, Daniel S. Homa, Gary R. Pickrell, Anbo Wang

***Abstract*— Modern high-temperature processes such as fossil energy production, nuclear reactors, and chemical reactors lack robust, distributed sensing systems to map temperatures in these high-value harsh-environment systems. Regular silica-fiber-based distributed temperature sensing (DTS) systems usually only operate at temperatures below about 800 °C. In this paper, we present the design, implementation, and testing of a distributed ultra-high temperature sensing system using Raman scattering intensity, which operates from room temperature to above 1400 °C. Consideration is given to the impacts of thermal radiation, fluorescence, and the multimode nature of unclad single-crystal fiber to optimize the system. Results from picosecond and sub-nanosecond lasers were compared. Measurements were taken with a ~2 m sapphire optical fiber; which represents the longest commercially available length. A spatial resolution of 12.4 cm and position standard deviation of 0.28 mm were achieved up to the maximum testing temperature of 1400 °C, which is a new record for distributed temperature sensing systems.**

***Index Terms*—Crystals, High-temperature, Optical fiber applications, Raman scattering, Time-domain analysis**

I. Introduction

Optical fiber temperature sensors have unique advantages over electronic sensors due to their electro-magnetic immunity, corrosion resistance, light weight, compact size, and the potential to measure multiple parameters simultaneously. The optical fiber sensor category can be divided into point sensors, quasi-distributed sensors, and fully distributed sensors. Point sensors using single-crystal fibers have been demonstrated to operate from room temperature up to 1800 °C with a temperature resolution of 1 °C using radiance or fluorescent lifetime detection methods [1, 2]. The most popular example of quasi-distributed sensing uses optical fiber Bragg gratings (FBG), which have been developed and used in industry for decades. Type I FBGs can work up to about 450 °C in silica fiber while type II gratings are stable at temperatures over 1000 °C but suffer from significant scattering loss [3]. Sapphire-fiber-based FBGs extend the sensing temperature to about 1400 °C [4-7]. Fully distributed temperature sensing (DTS) systems via silica fiber are already used in coal mine health monitoring [8], large oil tank reservoirs [9], and long-distance oil and gas pipe leak detection [10]. These DTS techniques are usually based on Rayleigh scattering, Brillouin scattering, or Raman scattering. Rayleigh-based optical frequency domain reflectometry (OFDR) offers the highest spatial resolution (down to the millimeter level) with limited sensing range (up to about several hundred meters) [11]. In some cases, combined methods may be adopted to extend the sensing range above 100 km [12]. Rayleigh and Brillouin based DTS systems are known for their multi-parameter sensing capabilities while Raman-based DTS systems are only sensitive to temperature, which eliminates interference from other changing parameters. All these systems are subject to trade-offs between sensing length and spatial resolution. In Raman based DTS systems, the spatial resolution is on the order of 1 meter when the total sensing length is over 10 km. The spatial resolution can however be improved to about ~1 centimeter via the use of ultra-short laser pulses and nanowire photodetectors [13]. Furthermore, Raman DTS measurements are commonly derived from the ratio of Stokes and Anti-Stokes signals, which cancels out the impacts of laser power fluctuations, varying coupling efficiency, and contamination of the fiber. This self-compensation further enhances long term measurement stability, making Raman preferable for distributed sensing in harsh environment applications.

Because silica glasses absorb other species, suffer dopant migration, and experience high-temperature deformation; silica fiber-based sensors can only work up to about 300 °C for longer periods of time in some harsh environment applications [14-

Manuscript received on August 10, 2018; accepted on xx xx, 2018. Date of publication xx xx, 2018; date of current version xx xx, 2018. (Corresponding author: Bo Liu.)

This technical effort was performed in support of the National Energy Technology Laboratory's research under the RES contract DE-FE0004000 and from work performed by Virginia Tech under financial assistance agreement DE- FE0012274.

Bo Liu was with Center for Photonics Technology, Virginia Tech, Blacksburg, VA, 24060 USA. He is now with National Energy Technology Laboratory and West Virginia University Research Cooperation, Morgantown, WV, 26505 USA. (E-mail: Bo.Liu@netl.doe.gov).

Michael P. Buric and Benjamin T. Chorpening are with National Energy Technology Laboratory, Morgantown, WV, 26505 USA (email: Michael.Buric@netl.doe.gov; Benjamin.Chorpening@netl.doe.gov).

Daniel S. Homa, Gary R. Pickrell, and Anbo Wang are with Center for Photonics Technology, Virginia Tech, Blacksburg, VA, 24060 USA. (e-mail: dan24@vt.edu; Pickrell@vt.edu; Awang@vt.edu).

Zhihao Yu was with Center for Photonics Technology, Virginia Tech, Blacksburg, VA 24061 USA. He is now with the College of Chemistry and Molecular Engineering, Peking University, Beijing, 100871 China (e-mail: zhihaoyu@pku.edu.cn).

16]. The maximum working temperature can be extended to about 700 °C with appropriate protection-layers, such as gold or aluminum [17]. These intermediate-temperature fibers are well suited for down-hole oil well monitoring. For the temperature regime above 800 °C, only single crystal fibers can survive longer periods. Single-crystal sapphire optical fibers have higher mechanical strength, laser damage threshold, power delivering capabilities, and better corrosion resistance than silica fibers. Unfortunately, most DTS methods that work well with silica fiber are not applicable, or exhibit significant performance degradation with multimode single-crystal fibers. Recently, Raman-based Optical Time Domain Reflectometry (OTDR) was demonstrated to work well at temperatures up to 1200 °C with an average temperature resolution of 3.7 °C and a spatial resolution of 14 cm [18]. Herein, the design details of this specific implementation will be discussed to provide future engineers the necessary tools to implement Raman DTS in single-crystal fibers.

There are two primary types of Raman DTS systems. The first (and most affordable) Raman DTS system utilizes a continuous-wave (CW) intensity-modulated laser and a photodetector. By monitoring the response of backward scattered light, the system can derive temperature information along the fiber using the inverse Fourier transform [19]. This method makes use of a low-coherence CW laser, and length information is derived from the response at different modulation frequencies. As a result, this method is also called Raman-based incoherent Optical Frequency Domain Reflectometry (RIOFDR). The second DTS method utilizes a pulsed laser to excite Raman scattering as the laser pulse propagates down the length of the test fiber. A time-history of the intensity of the backward scattered light is collected during a short measurement interval. The Raman Stokes band and Anti-Stokes band are selected and monitored by two identical photodetectors. Since the results are measured in the time domain, this method is usually known as Raman OTDR. The time-of-flight between the laser pulse and the collected scattering signal is related directly to the group velocity in the sensing optical fiber (SOF). In either Raman-based DTS system, the Raman scattering intensity is characterized by the Bose-Einstein statistics below in Eq. 1 and 2. Taking the ratio of the Stokes and Anti-Stokes radiated powers yields an expression which is invariant to the laser power (Eq. 3).

$$\left.\frac{d\sigma_{AS}}{d\Omega}\right|_x \cong \frac{1}{\lambda_{AS}^{\,4}} \frac{1}{\exp\left[\dfrac{hc\Delta\upsilon}{K_B T(x)}\right]-1} \tag{1}$$

$$\left.\frac{d\sigma_{S}}{d\Omega}\right|_x \cong \frac{1}{\lambda_{S}^{\,4}} \frac{1}{1-\exp\left[-\dfrac{hc\Delta\upsilon}{K_B T(x)}\right]} \tag{2}$$

$$R = \frac{I_{as}}{I_s} = \left(\frac{\upsilon_0+\Delta\upsilon}{\upsilon_0-\Delta\upsilon}\right)^4 \exp\left(-\frac{hc\Delta\upsilon}{K_B T(x)}\right) \tag{3}$$

where $\left.\frac{d\sigma_{AS}}{d\Omega}\right|_x$ and $\left.\frac{d\sigma_{S}}{d\Omega}\right|_x$ are the differential cross section of the AntiStokes component and Stokes components; λ_{AS} is the AntiStokes wavelength; λ_S is the Stokes wavelength; $\Delta\upsilon$ is the Raman shift; υ_0 is the frequency of the exciting light, T is the temperature; k_B is the Boltzmann constant, h is Planck constant, and c the speed of light in vacuum.

After choosing an appropriate method by which to construct a high-temperature distributed sensing system, it is necessary to design the system to perform well with single-crystal sapphire optical fiber. Although the fiber is capable of surviving the harsh environment, it presents some design challenges in implementing a working measurement system. Significant challenges exist in overcoming intense thermal radiation, small Raman collection efficiencies, and high modal volume for accurate measurement [20]. In this paper, we present the systematic design of sapphire fiber-based distributed ultra-high temperature sensing system via Raman scattering. Theoretical analysis and experimental results on the Raman gain, thermal radiation, and fluorescence are compared to optimize the system. Suggestions and perspective are proposed for the next generation DTS system.

II. System Design

The Raman DTS system is a pulsed, time-domain measurement system. A high power, short pulsed laser at 532 nm couples the light into the SOF, and the backward scattering is separated and monitored by two identical avalanche photodetectors (APD). A diagram of the Raman DTS system is illustrated in Fig. 1. The laser light first passes through a laser-line clean-up filter. A 50:50 beam splitter separates the laser beam into two beams of roughly equal power. The first beam is measured by a photodiode (PD), whose output serves as a trigger signal for data collection. The second beam is coupled into the SOF. The SOF is a commercially purchased single crystal sapphire fiber from Micromaterials, Inc. The backward scattering light from the SOF is reflected by the same beam splitter towards the detection system. Scattered light is first filtered by a stop-line filter (or Rayleigh filter), which removes light at the pump wavelength. A 770 nm edge blocking short-

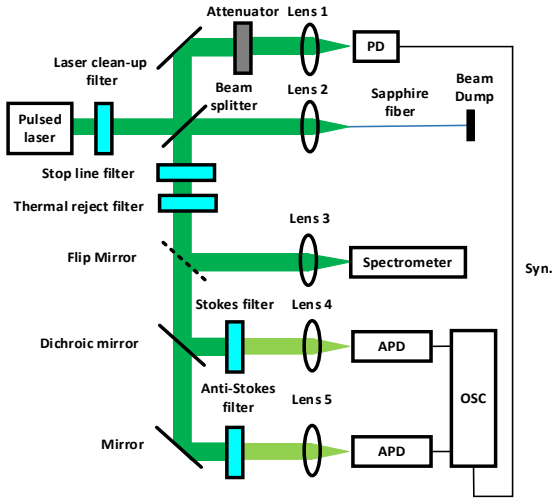

Fig. 1. Illustration of sapphire-fiber-based Raman DTS system (PD: photodetector; APD: Avalanche photodetector; OSC: Oscilloscope; PC: Computer; Syn.: Synchronization).

pass filter (Semrock, FF01-770/SP-25) serves as a thermal rejection filter to block the thermal radiation at longer wavelengths. A kinematic 2-position mirror (flip-mirror) is employed to permit periodic spectroscopic measurements using an auxiliary spectrometer. This permits careful characterization of thermal radiation or fluorescence in the system. With the flip-mirror in reflecting position, back-scattered light is coupled into the spectrometer. With the flip-mirror out of the way in non-reflecting position, the light is delivered to the remaining filters and APDs. Each APD receives a roughly ~25 nm wide portion of the spectrum centered at 520 nm and 543 nm respectively. This permits simultaneous measurement of the integrated Stokes and anti-Stokes radiation scattered by the fiber.

Although the system shown here is a free-space system and not a fiber-based system itself, a more commercially suitable configuration may ultimately be realized in an all-fiber configuration. Unfortunately, there are several fiber-optic component considerations that must be made before that implementation becomes possible. The main reason for use of a free space configuration is due to the huge Raman gain difference between common optical circulators and the single crystal fiber. The Raman scattering spectrum of silica-based graded-index fiber (GIF), silica-based step-index fiber (SIF), and sapphire fiber (SF) are excited with the same laser power and configurations indicated in Fig. 1. Their Raman spectra are compared in Fig. 2 with y-axis intensity normalized to the same fiber length. The sapphire fiber Raman gain is very weak compared to the amorphous silica-fiber Raman. In the figure, the intensity of sapphire fiber is multiplied by 10. The area under the Raman peak in graded-index silica fiber is about 100 times stronger than that in sapphire fibers, and 10 times stronger than that in step-index silica fiber, respectively. The Raman gain enhancement in graded-index multimode fiber is believed to be due to the Germanium dopant in the core [21]. Right now, most circulators are made of silica fiber, which will exhibit Raman signals much larger than those in sapphire fiber. If the single crystal is butt-coupled or spliced to a circulator, the sapphire fiber's Raman signal will be distorted upon detection due to the dead time effect of the APD [21]. In addition, most optical fiber circulators are designed for near-IR applications in telecom and exhibit high loss for visible light. Before an all-fiber configuration can be constructed, a visible-wavelength fiber circulator must be fabricated that can handle high peak powers and is designed for low-loss operation.

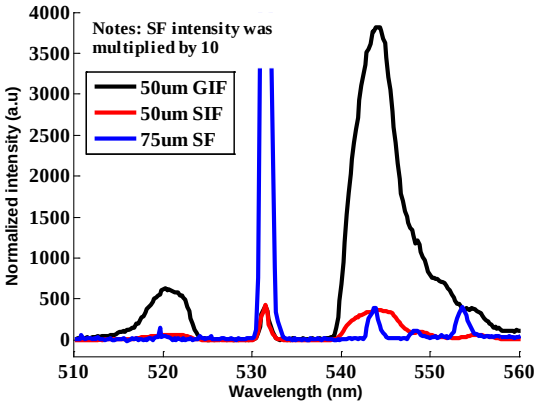

Fig. 2. Raman spectrums of 50μm core graded-index silica fiber (black), 50μm core step-index silica fiber (red), and 75μm core step-index sapphire fiber. The sapphire fiber spectrum intensity was multiplied by 10 for a better view.

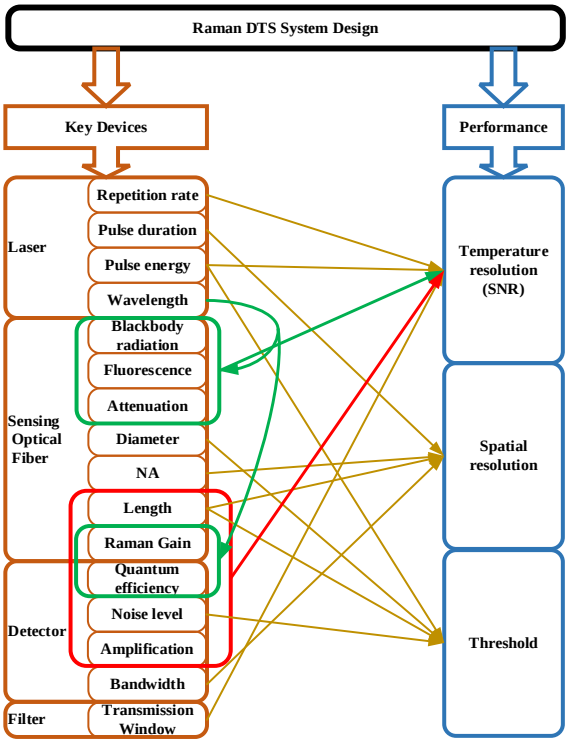

Fig. 3. Schematic relationship of Raman DTS system design in sensing optical fiber.

Alongside the beam-path consideration, construction of the Raman DTS system requires consideration of several other important aspects, which are summarized in Fig. 3. The key devices in the system to be specified include the laser, the measurement fiber or SOF, the detectors, and the filters. The performance parameters that will be affected by the choice of components include temperature resolution, spatial resolution, and detection limit. Each component exhibits certain parameters that will affect the performance of the system or affect the other system components. For example, the laser wavelength will determine the potential intensity of thermal radiation at the Stokes wavelength, the fluorescence intensity, the attenuation of the SOF, the Raman gain, and the quantum efficiency of the photodetector. In the following sub-sections, each of these design choices is discussed.

A. Pulse-width and Spatial Resolution

In choosing a laser pulse width, it is important to understand the physical phenomena governing the spatial resolution of measurements made using a time-domain measurement system. First, we define spatial resolution (as other DTS researchers have done [18, 21]) as the 10% to 90% response length. This is the distance over which light would travel in the SOF during the time taken for the detector to go from 10% to 90% of full scale in the presence of a perfect step function input to the fiber.

In a sapphire-fiber-based Raman DTS system, the spatial resolution δL_{SF} at fiber position L can be expressed as[22]:

$$\delta L_{SF} = \frac{c}{2n_{core}} t + L\left(\frac{1}{\sqrt{1-\left(\frac{NA}{n_{core}}\right)^2}} - 1\right) \quad (4)$$

where n_{core} is the refractive index of the fiber core, t is the laser pulse duration time (3 dB), and NA is the effective numerical aperture of the fiber.

The spatial resolution derived in Eq. 4 is composed of two terms. The first term is limited by the laser pulse duration time, while the second term is due to the pulse broadening in the multimode fiber. In graded-index multimode fibers, the second term is usually negligible because the graded-index profile eliminates the pulse broadening effect. However, this effect can be significantly larger in step-index fibers, such as the unclad sapphire fiber studied here. Examination of the equation leads one to believe that a high spatial resolution prefers the shortest possible laser pulse. In practice, the laser pulse duration time cannot be too small because a short pulse duration time implies a higher peak power at the same pulse energy. A higher peak power may easily damage the fiber end-facet. For bulk sapphire with laser wavelength at 532 nm and pulse duration time 50 ps, a fluence of about 9.3 J/cm^2 is required to induce damage [23]. Therefore, a laser pulse duration time from 100 ps to 1 ns is recommended to avoid the damage regime at reasonable power levels. The second term reveals that the spatial resolution is related to the numerical aperture (NA) and the measurement position (L) along the waveguide. The spatial resolution will decrease as the laser pulse propagates along the fiber due to the pulse broadening. Fig. 4(a) plots the relationship between spatial resolution, fiber length, and laser pulse duration in sapphire fiber with refractive index 1.774 at a laser wavelength of 532nm. The NA value in this simulation is 0.147 in a 125 μm commercial sapphire fiber. This may provide some confusion, as the NA for unclad sapphire optical fiber is not well defined. Observing the index difference between air and sapphire, we would believe that the NA of unclad sapphire is close to 1, which indicates transmission from any angle up to 90 degrees from the axial direction. In practice, transmission losses for higher order modes propagating at larger angles are much larger than the losses for lower-order modes. Therefore, the numerical aperture is continuously reduced with increasing fiber lengths, and some average numerical aperture must be considered for a particular configuration. Fig. 4(b) shows the relationship between the estimated spatial resolution and the NA of a 3-meter long fiber when a 0.7 ns laser pulse duration is used.

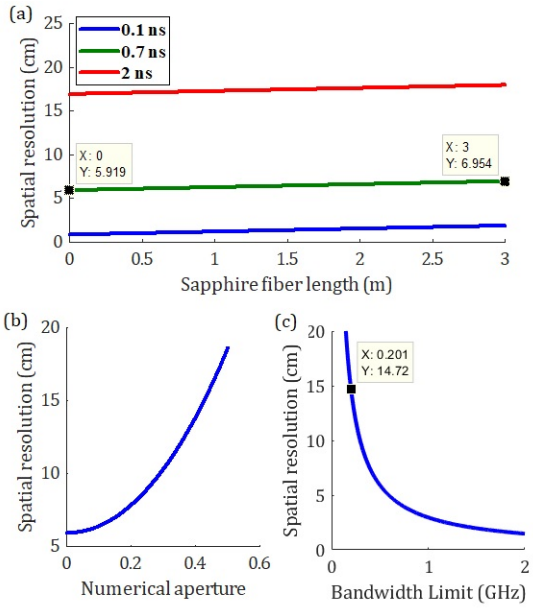

Fig. 4. Estimated spatial resolution of Raman DTS system. (a) Spatial resolution verses the sapphire fiber length and the laser pulse duration time (blue: 0.1ns; green: 0.7ns; red: 2ns); (b) Spatial resolution verses NA of the waveguide; (c) Spatial resolution verses bandwidth limit.

If we specify a laser pulse and a detector for a specific spatial resolution, we must also specify an electronic measurement system which records the APD signals that is capable of measuring at the same resolution. It is well known that the rising time of an oscilloscope approximately follows the rule:

$$t = \frac{0.35}{f_{Limit}} \quad (5)$$

The spatial resolution of the measurement system (ΔL) can be derived from the rising time as follow:

$$\Delta L = \frac{0.35}{f_{Limit}} \cdot \frac{c}{2n} \quad (6)$$

where f_{Limit} is the frequency-response limit of the slowest electrical component in the system, c is the speed of light in vacuum, and n is the refractive index of the fiber. In this calculation, we must consider the maximum frequencies of the APDs themselves, and the measurement oscilloscope; as the slowest component will ultimately limit the spatial resolution. Fig. 4(c) plots the relationship between the bandwidth of the electrical components and the measurable spatial resolution. Note that an approximately 500 MHz oscilloscope is capable of ~6 cm spatial resolution. The minimum spatial resolution in the system being designed is calculated to be ~3 cm, which is limited by APDs.

B. Laser Wavelength and Thermal radiation

Since the Raman DTS system is being designed for ultra-high temperature operation, the thermal radiation is a major challenge that will interfere with the detection of the Raman signal. Thermal radiation is intrinsic to all materials, and increases dramatically as the temperature increases. We usually begin to observe thermal radiation in hot objects (in a darkened room) at around 400 °C, with color and intensity changing to white hot near 1400 °C. Ideally, thermal radiation follows the thermal radiation function expressed by Planck's law [24]:

$$B(T) = \frac{2hc^2}{\lambda^5} \frac{1}{e^{\frac{hc}{\lambda k_B T}} - 1} \quad (7)$$

where B denotes spectral radiance, T is absolute temperature, λ is the wavelength. The actual thermal radiation observed also depends upon the emissivity of the material, which is often approximated as a constant over narrow ranges of wavelength.

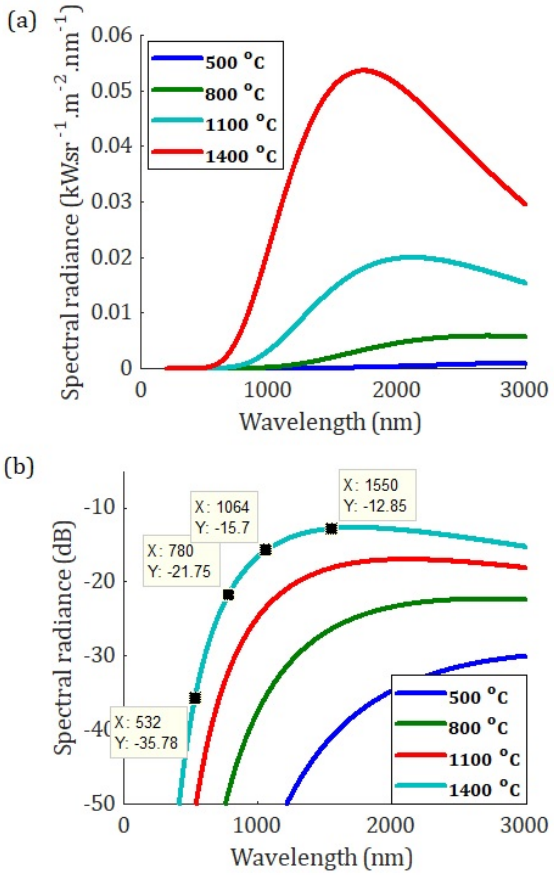

Fig. 5. Blackbody radiation at temperatures of interest. (a) Linear scale; (b) Log scale.

So, the observed thermal radiation follows the shape of the thermal function, but is somewhat less intense due to the non-ideal emissivity. The thermal function gives a maximum estimate for the thermal radiation.

Thermal radiation is usually normalized as spectral radiance per unit wavelength. The theoretical spectral radiances for objects at various temperatures are shown in Fig. 5. It shows that the peak of the thermal radiation is temperature dependent. This peak shifts towards shorter wavelengths at higher temperatures, indicating that shorter wavelength systems will experience less thermal interference. Researchers have demonstrated that a short wavelength pump-laser can effectively avoid most of the intense thermal radiation, enabling Raman measurements at high temperatures [25].

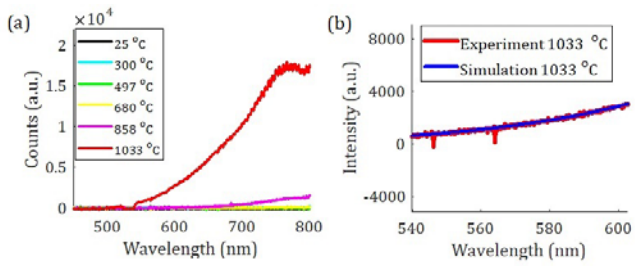

Fig. 6. (a) Spectral profile of the sapphire fiber thermal radiation at different temperatures; (b) Simulated and measured thermal radiation.

A brief heating experiment was carried out to verify the intensity of thermal radiation and determine the efficiency of the unclad sapphire fiber at collecting that thermal radiation and transmitting it to the detection system. A 75 µm diameter sapphire fiber was inserted into a tube furnace (MTI corporation, GSL1500X) and the temperature was increased while measuring the thermal emission at the other end of the fiber with a miniature spectrometer (Ocean Optics, USB4000). The measured thermal radiation spectrum is shown in Fig. 6(a). If we multiply a constant with the results derived from Planck's law (due to coupling efficiency and fiber loss), we find out that the simulation results and experimental results coincide very well (Fig. 6(b)). Both the theoretical and experimental results show that the thermal radiation is large at even modest furnace temperatures, and increases exponentially with wavelength and temperature. For example, the thermal radiation at 1550 nm is about 23 dB higher than that at 532 nm at 1400 °C. Therefore, successful Raman DTS operation will require short-visible wavelength lasers to measure the highest temperature range of interest.

C. Laser Wavelength and sapphire fluorescence

Our examination of thermal radiation-collection initially indicates that the laser wavelength should be near the blue/green end of the visible spectrum, but to more carefully specify an appropriate laser wavelength, we must consider the effects of fluorescence produced by the sapphire fiber itself. At temperatures above 1000 °C, thermal radiation is the major challenge, while fluorescence is usually of more concern at lower temperatures. Single crystal sapphire became very desirable after the invention of the first Ruby laser. The Ruby laser utilized a Cr^{3+} doped sapphire as the laser medium to produce light at ~694.3 nm. The Cr^{3+} dopant in sapphire was thereafter known to be a strongly-fluorescent dopant in this system. Although the level of Cr^{3+} impurities is relatively low in single crystal fibers made using Laser Heated Pedestal Growth, the fluorescence is often found to be stronger than Raman intensity [26, 27], depending on the exact fiber and experimental conditions. Using the Raman DTS system illustrated in Fig. 1, we can measure the relative amplitudes of the sapphire fiber Raman spectrum, the thermal radiation, and the fluorescence as the temperature is increased, which is shown in Fig. 7(a). The laser in this experiment is the Continuum SLIII-10 with its output wavelength at 532 nm. The laser pulse energy is about 500 µJ and the pulse width is about 24 ns. This experiment also shows that both thermal radiation and fluorescence can be several times higher than the sapphire Raman intensity. However, the laser wavelength at 532 nm effectively avoids both thermal radiation and fluorescence. By choosing this laser wavelength, the Stokes and Anti-Stokes bands overlap only the tail of the thermal and fluorescence peaks; which ensures minimal interference with detection of the Raman signals. From this figure, we can also conclude that any laser wavelength less than 540 nm or longer than 740 nm will avoid overlap with the fluorescence peak. Additionally, the thermal radiation at 740 nm is only about 10 times stronger than that at 532 nm. To compare the relative amplitude of sapphire Raman verses fluorescence, the thermal radiation background is recorded with laser light off and subsequently subtracted from the Raman spectrum, which is shown in Fig. 7(b). The interference pattern or ripples observed in that spectrum is a result of the multi-layer interference filters used to spectrally separate the collected light.

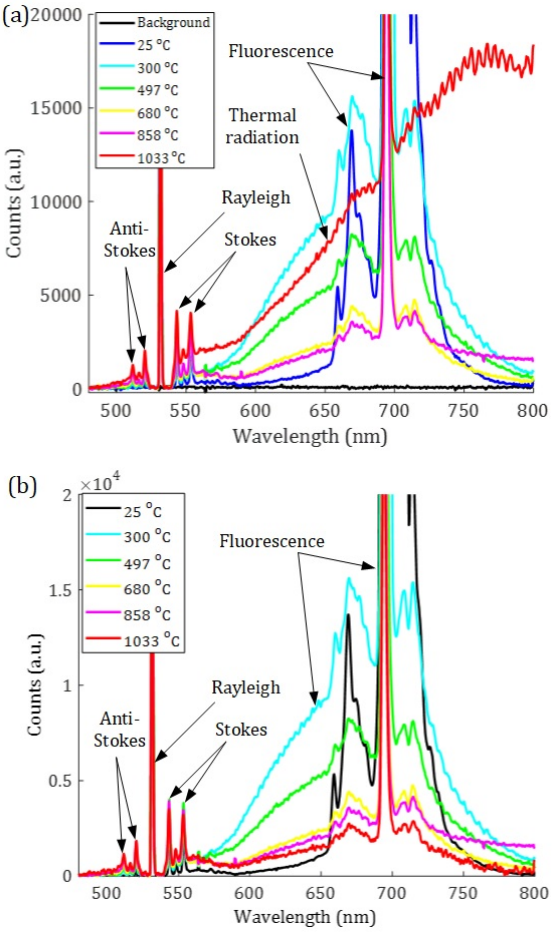

Fig. 7. (a) Sapphire fiber Raman spectrum, thermal radiation, and fluorescence at elevated temperatures. (b) Sapphire fiber Raman spectrum and fluorescence with thermal radiation background removed.

D. Optical filters

As we have shown, the collected Raman spectra in this application contains significant interference from fluorescence and thermal radiation. Because the Raman lines occur over a limited bandwidth region, while fluorescence and thermal radiation occupy much larger spectral regimes, it is highly advantageous to spectrally filter the collected light before it reaches the detection system. A well-designed set of filters should pass most or all of the Raman lines in sapphire and block the remainder of the spectrum. Sapphire has 7 well characterized Raman peaks at 379, 418, 431, 450, 578, 645 and 750 cm^{-1} [26, 28]. When the laser wavelength is chosen at 532 nm, some recommended optical filters and their pass windows are shown in Fig. 8.

Laser wavelength will also impact the choice of the optical filters because the Raman peak location and range is related to the laser wavelength. The relationship between laser wavelength, Raman Stokes wavelength, and Anti-Stokes wavelength is:

$$\lambda_{AS/S} = \frac{\lambda_0}{1 \pm \lambda_0 \cdot \Delta\omega} \tag{8}$$

where $\Delta\omega$ is the Raman shift, λ_0 is the laser wavelength, $\lambda_{AS/S}$ is the Raman Anti-Stokes or Stokes wavelength. For sapphire fibers, the shortest wavelength Raman peak is the 750 cm^{-1}

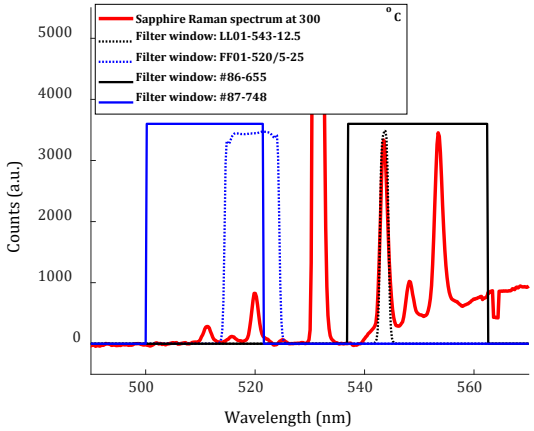

Fig. 8. Suggested band-pass optical filters (Semrock, LL01-543-12.5 & FF01-520/5-25; Edmund Optics, #86-655 & #87-748) for Raman DTS system when the laser wavelength is at 532nm.

Raman line on the Anti-Stokes side. The longest wavelength Raman peak is produced by the 750 cm^{-1} line on the Stokes side. Fig. 9(a) plots the position of the 418 cm^{-1} and 750 cm^{-1} peaks versus pump-laser wavelength. The total detection bandwidth (or span from the shortest wavelength Anti-Stokes peak to the longest wavelength Stokes peak) increases with the laser wavelength, and is shown in Fig. 9(b). We note that the detection bandwidth is only 42.6 nm at a laser wavelength of 532 nm, while the bandwidth increases to 365.6 nm when the laser wavelength is at 1550 nm.

E. General design conclusions

Component choices in a distributed Raman system ultimately play an important role in the operating characteristics of the complete measurement system. The choice in laser is indeed the foundation for many of the other component choices to be made upon. To summarize the previous sections, the appropriate pulse width is chosen with respect to the required spatial resolution, while the laser power is governed by the size of fiber and the damage threshold at a given pulse width. For a general-purpose measurement system with ~cm spatial resolution, we recommended a roughly 100-700 ps pulse with. For 125 μm sapphire fiber, we recommended a minimum pulse energy of 3 μJ. In determining a laser wavelength, we showed that a shorter wave pump will avoid common fluorescence problems, but that longer wave lasers can avoid the

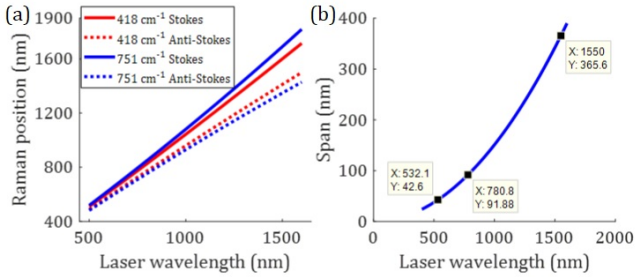

Fig. 9. (a)Raman peaks position of sapphire in wavelength domain; (b) Span of sapphire Raman peaks verse laser wavelength.

fluorescence issue, but will also experience too much thermal radiation. Thermal radiation ultimately drives the desire for shorter wave lasers, but the availability of detectors or reductions in detector quantum efficiency towards shorter wavelengths serve as limitations on how short a laser wavelength can ultimately be employed. The 532 nm wavelength used in the experimental system is a good compromise permitting accurate measurements over the desired temperature range.

III. Experiment

In the preliminary experiment, a diode-pumped solid-state laser (Passat Compiler) with ~5 ps pulse duration at 532 nm and 10 Hz was used. Although the maximum pulse energy of this laser was 120 µJ, only 3.75 µJ was coupled into the SOF to prevent the damage to the fiber end face. This energy corresponded to about 700 kW peak power, which was very close to the damage threshold at 5 ps. The optical bandpass filters in this experiment (Semrock, LL01-543-12.5 and FF01-520/5-25) only covered part of the Raman peaks, as was shown in Fig. 8 (dashed-line). The 750 cm^{-1} peaks were not collected for measurement. As long as the same portion of the Stokes and Anti-Stokes bands are collected, the ratio of those collected portions could still be used to accurately calculate the temperature. The SOF was a 96.5 cm long, 75 µm-diameter, single crystal sapphire fiber from Micromaterials, Inc. Both

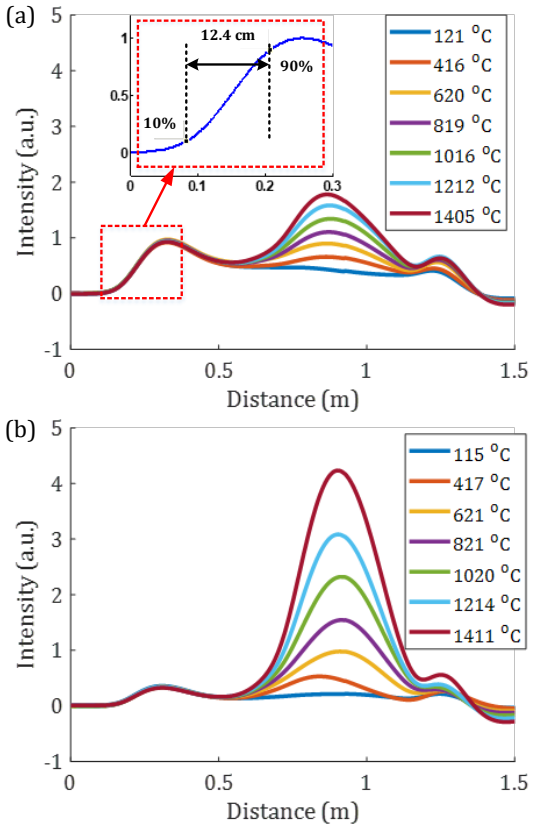

Fig. 10. The time-resolved Raman Stokes and Anti-Stokes signals along the optical sapphire fiber (b) Stokes; (c)Anti-Stokes.

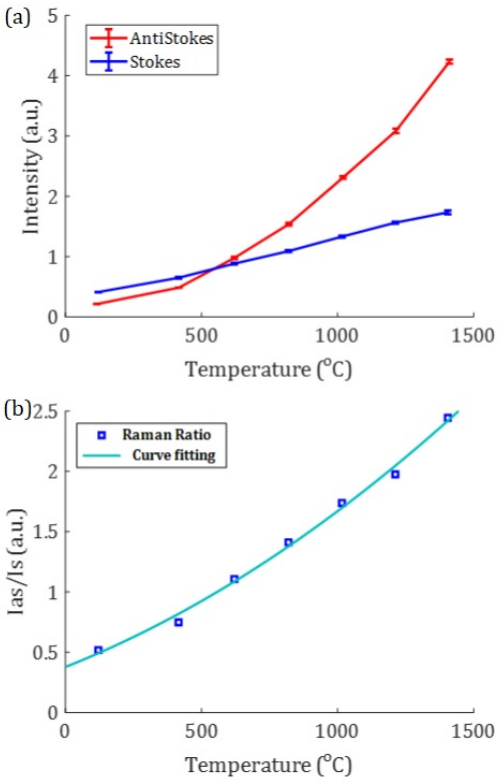

Fig. 11. (a) Stokes and Anti-Stokes signals at the center of the furnace; (b) Ration of Stokes to Anti-Stokes signals at the same location (~5ps laser pulse duration).

fiber end facets were polished to an 8-degree angle to minimize end reflections. The fiber's center section was placed in the furnace, and the furnace itself was carefully characterized using a thermocouple. To accomplish a comparable distributed measurement of the furnace profile, a B-type thermocouple was translated through the furnace at each temperature setting. Once the furnace temperature profile was established independently, the furnace was ramped up to 1400 °C in small increments, recording the Raman-derived temperature profile at each step. Fig. 10(a) and Fig. 10(b) plot the integrated Stokes and Anti-Stokes band intensities over time via the APD signals.

The Raman peak intensities at the center of the hot-zone are plotted in Fig. 11(a) and the corresponding Raman ratio is plotted in Fig. 11(b). The ratio is then approximated as a 2nd order equation via curve fitting. The error between experiment points and the curve fitting are due to a combination of furnace innacuracy and optical noise (fluorescence and thermal).

After successfully establishing operation with the picosecond laser, a more complete experiment was carried out with a sub-nanosecond laser. This laser is a Passively Q-switched microchip laser at 532 nm. The maximum pulse energy was ~5 µJ at 10 Hz and the pulse duration time was about 700 ps. Since the pulse duration time is much longer than the pico-second laser, the calculated peak power (~7 kW) was about 100 times smaller than the laser power used in the preliminary experiment. This low peak power ensured that the sapphire fiber was not damaged, even in the event of poor alignment. To allow more Raman peaks to be collected, a wider window band-pass filter was installed in the system (Edmund Optics, #86-655 and #87-748). The transmission spectrum of

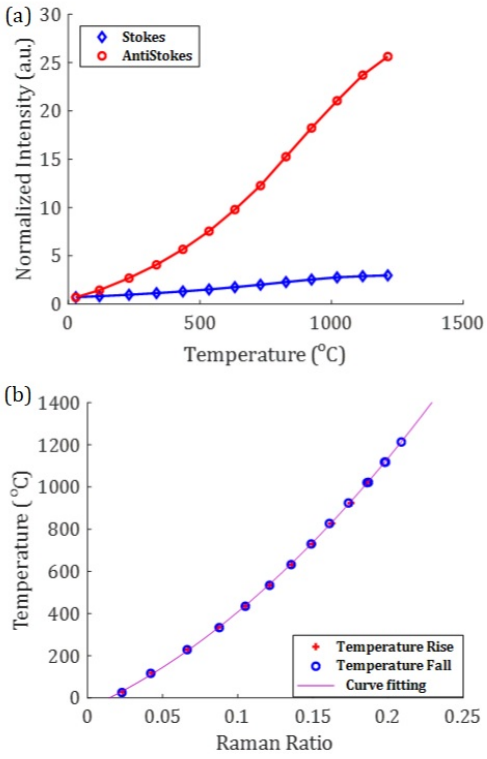

Fig. 12. (a)Raman signals verses temperature at the heating center; (b) Raman ratio verses temperature at the heating center (700ps laser pulse duration).

this wider band filter was about 25 nm and was plotted in Fig. 8. To measure the furnace temperature more accurately, a K-type thermocouple was used, which limited the furnace operation to about 1200 °C. The Stokes and Anti-Stokes signals

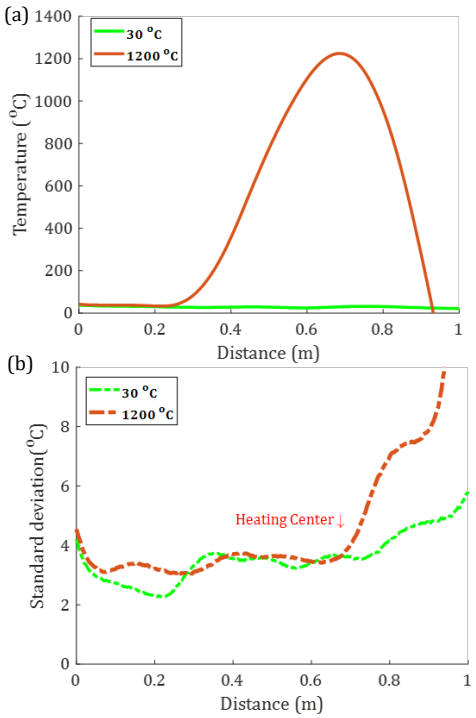

Fig. 13. (a)Demodulated temperature profile along the fiber; (b)Corresponding standard deviation.

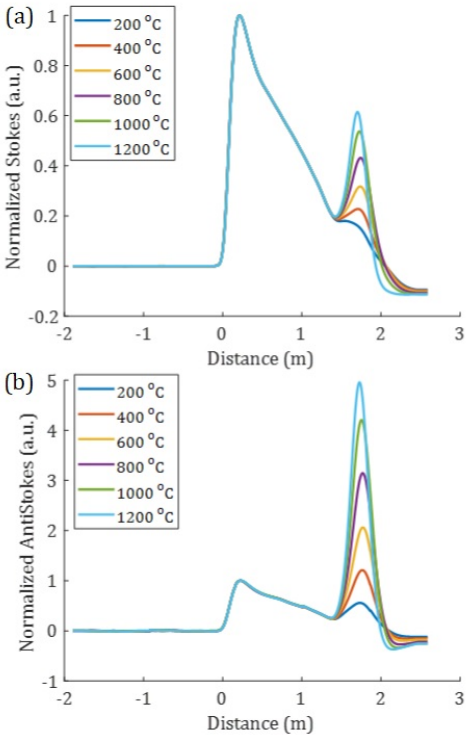

Fig. 14. Raman signals using a 2-meter long sapphire fiber Raman (a)Stokes and (b)Anti-Stokes response at elevated temperatures.

at the heating center versus temperature are plotted in Fig. 12(a) and the corresponding Raman ratio is plotted in Fig. 12(b) versus the temperature, along with the fitted curve which will be used to approximate the temperature being measured. With a wider band-pass window, the signal intensity is much larger than in the previous experiment.

After deriving the function for the temperature vs. Raman ratio, it is possible to demodulate the recorded ratios into complete temperature profiles. The demodulated temperature profiles between 30 °C and 1200 °C are plotted in Fig. 13(a) and the standard deviations are shown in Fig. 13(b). It shows that the measurement accuracy does not degrade at high temperatures. The average standard deviation at the heating center is 3.7 °C with error increasing toward the end of the measurement fiber.

The same experiment was carried out on a 2-meter long sapphire fiber. The Raman Stokes and Anti-Stokes signal are shown in Fig. 14.

Next, during a period of 3 days, the furnace temperature was slowly raised and lowered again while comparing the Raman and thermocouple-based measurements. There was one instance where the thermocouple displayed erroneous measurements while the Raman based measurement was stable and correct. These measurements are shown in Fig. 15. It is likely that this was due to contamination of the thermocouple or symptoms of the thermocouple junction beginning to fail. This further illustrated the utility of measurement made using the highly stable sapphire fiber.

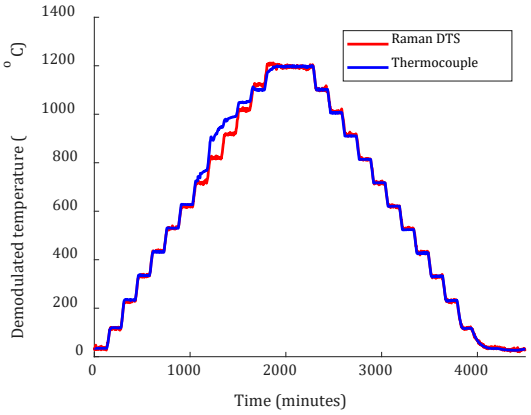

Fig. 15. Raman DTS system results verses thermal coupling reading during a temperature cycle experiment.

Finally, a spatial resolution test was designed to show that despite the smooth continuous profile, the system is indeed measuring the correct temperature at each location. To demonstrate the spatial resolution, a 1.6-meter long sapphire fiber was placed in a tube furnace and heated to 500 °C. One end of the sapphire fiber was mounted on a translation stage. The translation stage dragged the fiber through the furnace axially in 1cm increments over a total range of 13 cm. The Raman ratio was monitored at each different location and the temperature profile was derived. Fig. 16 Shows that the temperature profile moved in 1cm increments; accurately measuring the profile with position accuracy of 280 µm (standard deviation). The response of the unheated fiber section remains the same while the heated sections moves with the fiber position.

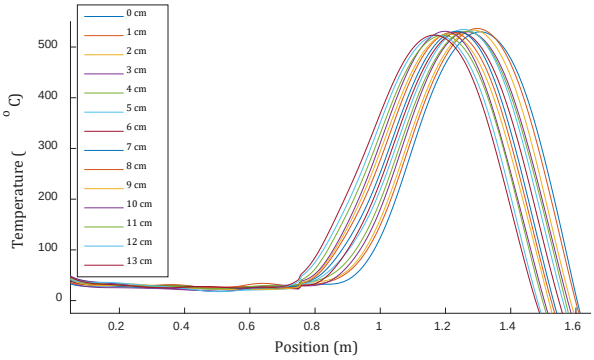

Fig. 16. Position accuracy measured through fiber translation.

IV. Perspective and Conclusions

There is a significant and immediate need for distributed temperature sensing at high-temperatures in a number of industries including power generation, transportation, and chemical production. To fill this need, we have proposed a sapphire-fiber based distributed temperature sensing system employing Raman scattering to derive temperature information. The system is intended for use in high-value applications like turbine engines, nuclear power plants, and chemical production reactors. Although we have demonstrated the operational capabilities of the measurement system in its present rudimentary state, several improvements can be made that will ultimately make the system more robust and field-worthy.

In order to ruggedize the measurement system, it is desirable to pursue an all-fiber solution that would eliminate bulky and mis-alignment prone free-space components. This will permit integration with systems like aviation turbines or other flight or G-rated systems. To eliminate the free space coupling components, one will need to invent a specialized optical circulator which will not employ silica, or any other material with a large Raman gain that will obscure the smaller Raman signals from the single-crystal fiber. Along the same lines, if the sensing fiber is to be placed in a remote location away from the interrogator, a long length of lead-in fiber will be required. This fiber must exhibit good coupling capabilities with the SOF, and a low Raman gain to avoid the APD dead-time effect.

Another valuable research direction is to use other single crystal fibers or doped crystal fibers as the sensing waveguide in place of sapphire fiber. Yttrium aluminum garnet (YAG) fiber is a good alternative candidate to sapphire fiber due to the high melting point (1940 °C), similar chemical resistance, and higher Raman gain. YAG fibers can be doped with a broad range of rare earth dopants or other materials with larger Raman cross sections. GeO_2 is a good dopant candidate for this task due to its high Raman gain. Once a high Raman gain single crystal fiber is produced, it may be possible to use a regular silica fiber circulator and silica lead-in fiber.

The most valuable but perhaps the most challenging aspect to be investigated is the cladding of single-crystal fibers for high-temperature, low-loss operation. A cladded crystal fiber will reduce the fiber numerical aperture (NA) and reduce the number of modes in the fiber; resulting in a less laser pulse broadening and better spatial resolution. It will also help protect the fiber from contamination in the harsh measurement environment. This will also likely increase the longevity of the sensing fiber and increase overall measurement stability over time.

In summary, we have demonstrated a sapphire-fiber-based, fully distributed, ultra-high temperature sensing system via Raman scattering. The system was shown to operate from room temperature up to 1400 °C with a 3.7 °C average standard deviation at the center of the hot zone. A systematic review of the design aspects shows that a 1 cm long theoretical spatial resolution is possible. Laser wavelengths between 500-600 nm and 740-1000 nm are good choices to avoid the intense fluorescence at 694.3 nm. Use of shorter wavelengths avoids the high-temperature thermal radiation induced in the fiber. The Raman DTS system showed better stability than a K-type thermocouple measurement in a three-day temperature ramp experiment reaching 1200 °C. Comparison with a translated-fiber temperature measurement showed a position accuracy of <1 mm was achieved. A higher signal to noise ratio is easily achievable with the implementation of higher laser pulse energy and repetition rate. Future iterations of the sensing system will include further improvements in field-readiness, packaging, and overall performance. With these iterations, we hope to produce an industrially viable measurement system for currently inaccessible measurement opportunities that will aid in the control of industrial processes, as well as serving in the

toolkit of other scientists and researchers on the forefront of modern technologies.

DISCLAIMER

This project was funded by the Department of Energy, National Energy Technology Laboratory, an agency of the United States Government, through a support contract with AECOM. Neither the United States Government nor any agency thereof, nor any of their employees, nor AECOM, nor any of their employees, makes any warranty, expressed or implied, or assumes any legal liability or responsibility for the accuracy, completeness, or usefulness of any information, apparatus, product, or process disclosed, or represents that its use would not infringe privately owned rights. Reference herein to any specific commercial product, process, or service by trade name, trademark, manufacturer, or otherwise, does not necessarily constitute or imply its endorsement, recommendation, or favoring by the United States Government or any agency thereof. The views and opinions of authors expressed herein do not necessarily state or reflect those of the United States Government or any agency thereof.

REFERENCES

[1] Z. Tian, Z. Yu, B. Liu, and A. Wang, "Sourceless optical fiber high temperature sensor," *Opt Lett*, vol. 41, pp. 195-198, Jan 15 2016.

[2] Y. Shen, L. Tong, Y. Wang, and L. Ye, "Sapphire-fiber thermometer ranging from 20 to 1800 °C," *Appl Optics*, vol. 38, pp. 1139-1143, Mar 1 1999.

[3] S. J. Mihailov, "Fiber Bragg Grating Sensors for Harsh Environments," *Sensors*, vol. 12, p. 1898, 2012.

[4] S. Yang, D. Homa, G. Pickrell, and A. Wang, "Fiber Bragg grating fabricated in micro-single-crystal sapphire fiber," *Opt Lett*, vol. 43, pp. 62-65, Jan 1 2018.

[5] S. Yang, D. Hu, and A. Wang, "Point-by-point fabrication and characterization of sapphire fiber Bragg gratings," *Opt Lett*, vol. 42, pp. 4219-4222, Oct 15 2017.

[6] T. H. Tino Elsmann, Albrecht Graf, Manfred Rothhardt, Markus A. Schmidt, Hartmut and Bartelt, "First-order sapphire fiber Bragg gratings for high temperature sensing," *GMA/ITG-Fachtagung Sensoren und Messsysteme*, 2016, pp. 53-58.

[7] S. J. Mihailov, "Fiber Bragg grating sensors for harsh environments," *Sensors (Basel)*, vol. 12, pp. 1898-918, 2012.

[8] Y. Liu, T. Lei, Y. Wei, Z. Sun, C. Wang, and T. Liu, "Application of Distributed Optical Fiber Temperature Sensing System Based on Raman Scattering in Coal Mine Safety Monitoring," in *2012 Symposium on Photonics and Optoelectronics*, 2012, pp. 1-4.

[9] J. M. D. Freitas, "Recent developments in seismic seabed oil reservoir monitoring applications using fibre-optic sensing networks," *Meas Sci Technol*, vol. 22, p. 052001, 2011.

[10] D. Inaudi and B. Glisic, "Long-range pipeline monitoring by distributed fiber optic sensing," *J Press Vess-T Asme*, vol. 132, p. 011701, 2010.

[11] M. E. Froggatt, D. K. Gifford, S. T. Kreger, M. S. Wolfe, and B. J. Soller, "Distributed strain and temperature discrimination in unaltered polarization maintaining fiber," in *P Soc Photon-Opt Ins*, 2006, p. ThC5.

[12] M. N. Alahbabi, Y. T. Cho, and T. P. Newson, "150-km-range distributed temperature sensor based on coherent detection of spontaneous Brillouin backscatter and in-line Raman amplification," *J Opt Soc Am B*, vol. 22, pp. 1321-1324, Jun 2005.

[13] M. G. Tanner, S. D. Dyer, B. Baek, R. H. Hadfield, and S. Woo Nam, "High-resolution single-mode fiber-optic distributed Raman sensor for absolute temperature measurement using superconducting nanowire single-photon detectors," *Appl Phys Lett*, vol. 99, p. 201110, 2011.

[14] G. R. Pickrell, Y. Duan, B. Qi, R. G. May, and A. Wang, "Diffusion of water in optical fibers at elevated temperature and pressure," in *P Soc Photo-Opt Ins*, 2002, pp. 239-251.

[15] Z. Huang, G. R. Pickrell, and A. Wang, "Penetration rate of water in sapphire and silica optical fibers at elevated temperature and pressure," *Opt Eng*, vol. 43, pp. 1272-1274, 2004.

[16] L. Yu, E. Bonnell, D. Homa, G. Pickrell, A. Wang, P. Ohodnicki Jr, *et al.*, "Observation of temperature dependence of the IR hydroxyl absorption bands in silica optical fiber," *Opt Fiber Technol*, vol. 30, pp. 1-7, 2016.

[17] M. Farhadiroushan, T. R. Parker, and M. Mondanos, "Sensing system using optical fiber suited to high temperatures," ed: Google Patents, 2011.

[18] B. Liu, Z. Yu, C. Hill, Y. Cheng, D. Homa, G. Pickrell, *et al.*, "Sapphire-fiber-based distributed high-temperature sensing system," *Opt Lett*, vol. 41, pp. 4405-8, Sep 15 2016.

[19] E. Karamehmedović, *Incoherent optical frequency domain reflectometry for distributed thermal sensing*: COM, DTU, 2007.

[20] M. Buric, B. Liu, S. Huang, M. Wang, K. Chen, P. Lu, *et al.*, "Modified single crystal fibers for distributed sensing applications," in *Fiber Optic Sensors and Applications XIV*, 2017, p. 102080C.

[21] M. Höbel, J. Ricka, M. Wüthrich, and T. Binkert, "High-resolution distributed temperature sensing with the multiphoton-timing technique," *Appl Opt*, vol. 34, pp. 2955-2967, Jun 1 1995.

[22] B. Liu, "Sapphire Fiber-based Distributed High-temperature Sensing System," Ph.D. dissertation, Electric and Computer Engineering, Virginia Tech, Blacksburg, 2016.

[23] B. Bussiere, O. Uteza, N. Sanner, M. Sentis, G. Riboulet, L. Vigroux, *et al.*, "Bulk laser-induced damage threshold of titanium-doped sapphire crystals," *Appl Opt*, vol. 51, pp. 7826-7833, 2012.

[24] M. Planck, *The theory of heat radiation*: Courier Corporation, 2013.

[25] E. Zouboulis, D. Renusch, and M. Grimsditch, "Advantages of ultraviolet Raman scattering for high temperature investigations," *Appl phys lett*, vol. 72, pp. 1-3, 1998.

[26] B. Liu, Z. Yu, Z. Tian, D. Homa, C. Hill, A. Wang, *et al.*, "Temperature dependence of sapphire fiber Raman scattering," *Opt Lett*, vol. 40, pp. 2041-2044, May 1 2015.

[27] C. Raml, X. He, M. Han, D. R. Alexander, and Y. Lu, "Raman spectroscopy based on a single-crystal sapphire fiber," *Opt Lett*, vol. 36, pp. 1287-9, Apr 01 2011.

[28] J. Thapa, B. Liu, S. D. Woodruff, B. T. Chorpening, and M. P. Buric, "Raman scattering in single-crystal sapphire at elevated temperatures," *Appl Opt*, vol. 56, pp. 8598-8606, Nov 1 2017.